Bull. Mater. Sci. (2023)46:62
https://doi.org/10.1007/s12034-023-02896-5

Influence of surfactant on the structural, morphological and optical properties of $SrWO_4$: Insights through electron density distribution analysis

SANTHANAM BALU[1], D SIVAGANESH[1], S SARAVANAKUMAR[1,*], V SIVAKUMAR[2], JI-MAN KIM[3], PADMANATHAN KARTHICK KANNAN[3,*] and V GANESH[4]

[1] International Research Centre, Department of Physics, Kalasalingam Academy of Research and Education, Virudhunagar 626126, India

[2] Department of Physics, M. Kumaraswamy College of Engineering, Karur 639113, India

[3] Department of Chemistry, Sungkyunkwan University, Suwon 16419, Republic of Korea

[4] Advanced Functional Materials and Optoelectronic Laboratory, Faculty of Science, Department of Physics, King Khalid University, P.O. Box 9004, Abha, Saudi Arabia

*Author for correspondence (saravanaphysics@gmail.com; pkk.matsci@gmail.com)

MS received 21 September 2022; accepted 16 November 2022

Abstract. Scheelite-type surfactant-assisted $SrWO_4$ was prepared via a simple co-precipitation method. The effect of various surfactants such as hexamethylenetetramine, polyvinylpyrrolidone, and sodium dodecyl sulphate, on the structural, morphological and photoluminescence (PL) properties of $SrWO_4$ was investigated. Powder X-ray diffraction and the Rietveld profile refinement technique confirmed the tetragonal structure of all the as-synthesized $SrWO_4$ materials. Among the three surfactants, particles with spherical morphology were observed for SDS-assisted $SrWO_4$. Surfactant-assisted $SrWO_4$ exhibited bluish-green emission around 500 nm, ascribed to the presence of $\left(WO_4^{2-}\right)$ luminescence centre at 284 nm excitation, and the PL emission intensity significantly increased in the presence of surfactant. Electron density distribution analysis of a single unit cell for all the prepared materials was investigated, and correlated with the PL results.

Keywords. Surfactant; Rietveld analysis; PL studies; electron density distribution; luminescence centre.

1. Introduction

It is well-known that lighting is very essential in the current era. Many researchers have developed various lamp sources such as candles, oil lamps, halogen lamps, incandescent lamps, mercury lamps and fluorescent lamps [1]. However, conventional light sources have limitations, such as huge energy consumption, minimum lifespan, low luminous efficacy and carbon dioxide emission (CO_2) that highly affect the ecosystem [2]. In contrast, white light-emitting diodes are highly beneficial compared to conventional light sources because of their low power consumption at luminance, long lifespan, high luminous efficiency and eco-friendly [3, 4]. Hence, it is essential to develop white LED with high luminous efficiency.

To date, many number of inorganic phosphor materials such as oxides, nitrides, silicate, borates, aluminates and tungstates are used for the white light emission in light-emitting diodes [5]. Among them, tungstate materials find potential attention in energy and environmental applications owing to their excellent physical, chemical and thermal properties [6]. Mainly, $SrWO_4$ is of great interest in scintillation detectors, optical fibres, microwave applications, optoelectronic devices, light-emitting devices due to its unique optical, magnetic, electrical and thermal properties [7].

In general, a few parameters such as crystallinity, surface morphology and particle size highly influence the light-emitting properties of a luminescent material [8, 9]. There have been many papers reported on the synthesis of $SrWO_4$ with high crystallinity and well-defined surface morphology using diverse preparation methods such as co-precipitation [10], hydrothermal [11], sol–gel [12], wet chemical [13], polyol [14], solid-state reaction [15] and surfactant-assisted [16] methods. Though each method has specific advantages and limitations on the properties of a material, the presence of surfactant during synthesis can enhance their physicochemical properties [17]. Surfactant plays vital role in controlling the synthesis of materials, as they tend to decrease the agglomeration of nanoparticles and increase the crystallinity with uniform morphology [18, 19].

Published online: 28 March 2023

Recently, Swathi *et al* [20] reported the hydrothermally synthesized pristine and cetyl trimethyl ammonium bromide-assisted tungsten sulphide (WS_2), in which surfactant-assisted WS_2 showed 90% retention in a 16-h catalytic activity test with enhanced stability. In another report, hydrothermally synthesized WO_3 nanostructures were used for dye-sensitized solar cell application, in which the incorporation of sodium dodecyl sulphate (SDS) during WO_3 synthesis had greatly influenced the surface microstructure, resulting in enhanced photo-conversion efficiency [21]. Another study showed the effect of surfactant on the photo-electrocatalytic activity of $ZnWO_4$, in which three different kinds of surfactants viz. ethylene glycol, cetyl trimethyl ammonium bromide and sodium dodecyl benzene sulphonate were used for the synthesis of monoclinic $ZnWO_4$ through hydrothermal technique. From their report, it is found that surfactant is highly influencing the microstructure and morphology of $ZnWO_4$ [22]. Tian *et al* [16] reported the optical properties of $SrWO_4$ materials prepared through a hydrothermal route using cetyl trimethyl ammonium bromide surfactant.

By keeping these facts as a motivation, in this work, an attempt has been made to prepare $SrWO_4$ in the presence of three different surfactants such as hexamethylenetetramine (HMTA), polyvinylpyrrolidone (PVP) and sodium dodecyl sulphate (SDS) using co-precipitation method. The detailed structural information is very much essential for the fabrication of a sensible device. An electron density distribution analysis [20–24] for the $SrWO_4$ material has been carried out by extracting the in-depth local structure information along with bonding properties. In order to get the in-depth information about the luminescent properties of the $SrWO_4$ samples, an investigation has been made by correlating the obtained PL data with the electron density distribution analysis.

2. Experimental

2.1 *Materials*

Strontium nitrate ($(Sr(NO_3)_2$, 99% AR grade purchased from LOBA) and 99% AR grade of sodium tungstate ($Na_2WO_4{\cdot}2H_2O$, purchased from LOBA) were used as starting precursors. Hexamethylenetetramine ($C_6H_{12}N_4$), polyvinylpyrrolidone ($(C_6H_9NO)n$) and sodium dodecyl sulphate ($NaC_{12}H_{25}SO_4$) were purchased from Merck and used as-received.

2.2 *Sample preparation*

$SrWO_4$ material was synthesized using a co-precipitation method. At first, equimolar concentration of $Sr(NO_3)_2$ (2.1163 g) and $Na_2WO_4{\cdot}2H_2O$ (3.298 g) were dissolved in 100 ml of deionized (DI) water separately. Similarly, surfactant solutions were prepared by mixing the appropriate quantity (above critical micelle concentration) of three different surfactants viz. HMTA, PVP and SDS in 100 ml DI under stirring condition. $Na_2WO_4{\cdot}2H_2O$ and surfactant solutions were simultaneously added dropwise to the solution of $Sr(NO_3)_2$ and continuously stirred for 1 h. A clear white precipitate is formed during the reaction. The white precipitate was gently extracted by centrifugation process and thoroughly washed multiple times using ethanol and DI. After that, the samples were dried at 120°C for 5 h. The dried sample was calcinated at 700°C in air for 3 h to obtain a surfactant-assisted $SrWO_4$ material. The $SrWO_4$ samples obtained using HMTA, PVP and SDS were henceforth designated as $SrWO_4$:HMTA, $SrWO_4$:PVP and $SrWO_4$:-SDS, respectively. The schematic representation of the

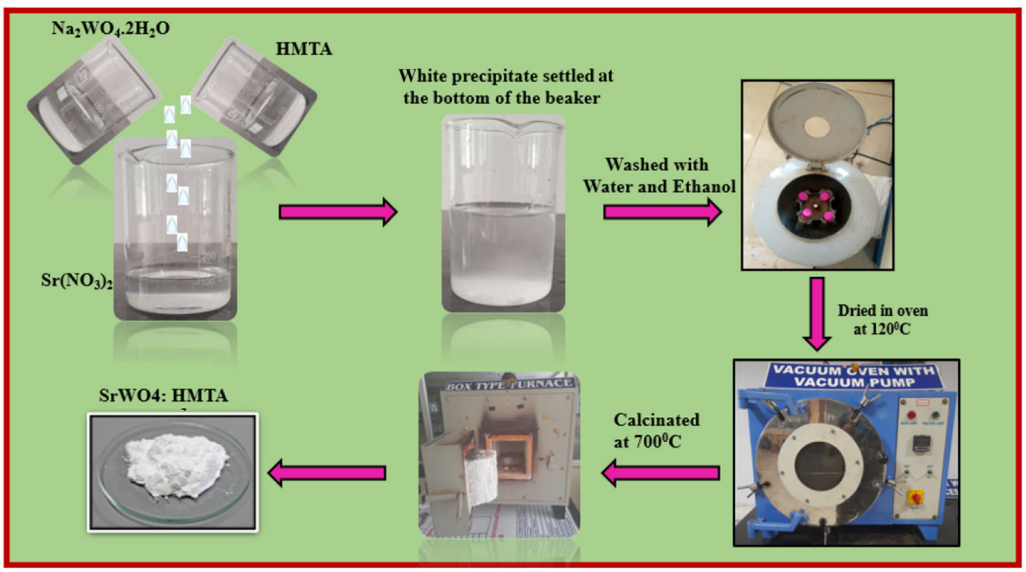

Scheme 1. The experimental procedure for the synthesis of HMTA-assisted $SrWO_4$ (similar procedure is adapted for the synthesis of other surfactant-assisted samples).

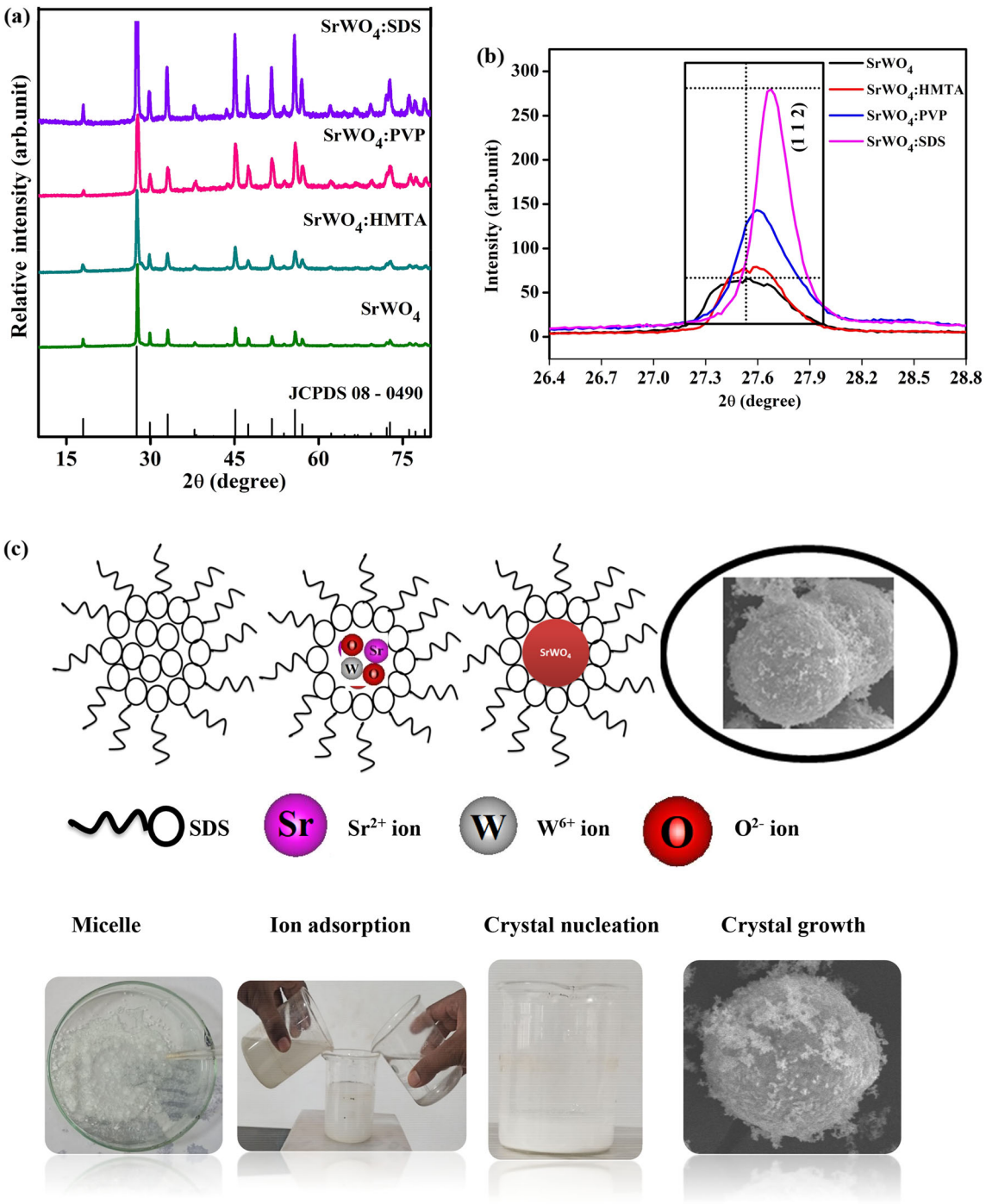

Figure 1. (**a**) PXRD profiles of $SrWO_4$ materials. (**b**) Enlarged diffraction pattern on (112) plane of $SrWO_4$ materials. (**c**) Growth mechanism of SDS-assisted synthesis of $SrWO_4$.

preparation of HMTA-assisted $SrWO_4$ is shown in scheme 1.

2.3 *Sample characterization*

The crystallinity of the synthesized materials was determined using a Bruker D8 advanced ECO X-ray diffractometer employing CuK_α radiation with a step size of 0.02° in the 2θ range of 10–80°. A scanning electron microscope (SEM; ZEISS-Sigma 300 microscope) and an energy dispersive X-ray spectrometer (HORIBA EMAX X-ACT) were used to analyse the surface morphology and elemental composition of the as-synthesized material, respectively. The photoluminescence (PL) spectrum of all materials was recorded using a Jobin Yvon Fluoromax-4C

Table 1. Refined structural parameters of $SrWO_4$ materials.

Parameters/materials	$SrWO_4$	$SrWO_4$:HMTA	$SrWO_4$:PVP	$SrWO_4$:SDS
$a = b$ (Å)	5.4360 (7)	5.4201 (8)	5.3930 (3)	5.3915 (9)
c (Å)	12.0027 (3)	11.9656 (8)	11.9131 (8)	11.8999 (12)
$\alpha = \beta = \gamma$ (°)	90	90	90	90
Volume $(Å)^3$	354.59 (3)	351.32 (1)	346.41 (2)	345.49 (1)
Density (g cm^{-3})	6.28	6.34	6.43	6.44
R_{obs} (%)	2.21	2.28	2.31	2.33
R_p (%)	4.95	5.12	5.34	5.22
GOF	0.21	0.22	0.23	0.23

R_{obs}, reliability index for observed structure factors; R_P, reliability index for profile; GOF, goodness of fit.

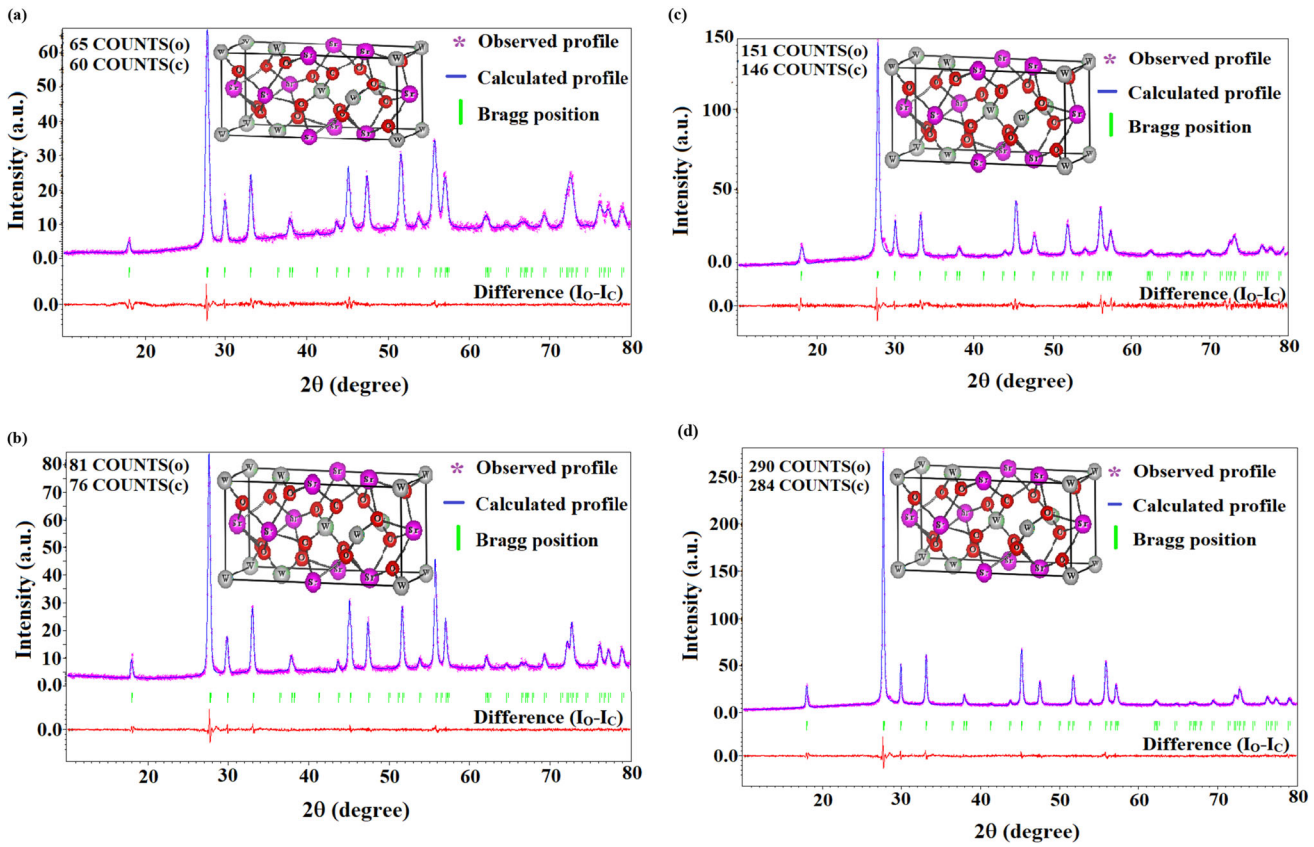

Figure 2. Rietveld refinement profiles of (**a**) $SrWO_4$, (**b**) $SrWO_4$:HMTA, (**c**) $SrWO_4$:PVP and (**d**) $SrWO_4$:SDS.

Spectrofluorometer by employing 150W Xenon lamp as an excitation source.

3. Results and discussions

3.1 *Structural analysis*

Figure 1a shows the observed powder X-ray diffraction (PXRD) patterns of all the surfactant-assisted $SrWO_4$ materials. The pure phase of tetragonal-structured $SrWO_4$ was observed for all the samples in the space group of I41/a and confirmed with the standard JCPDS pattern [7]. No additional peaks were observed in the observed XRD profiles, suggesting the high purity of the prepared materials.

Figure 1b shows the enlarged diffraction pattern on (112) plane of all the samples. Of all the surfactants, $SrWO_4$:SDS material showed maximum intensity indicating their high crystallinity than that of other surfactant-assisted $SrWO_4$ materials. In addition to that, the diffraction angle was shifted towards higher value of 2θ, as observed in figure 1b, showing that the unit cell is of more compressive nature

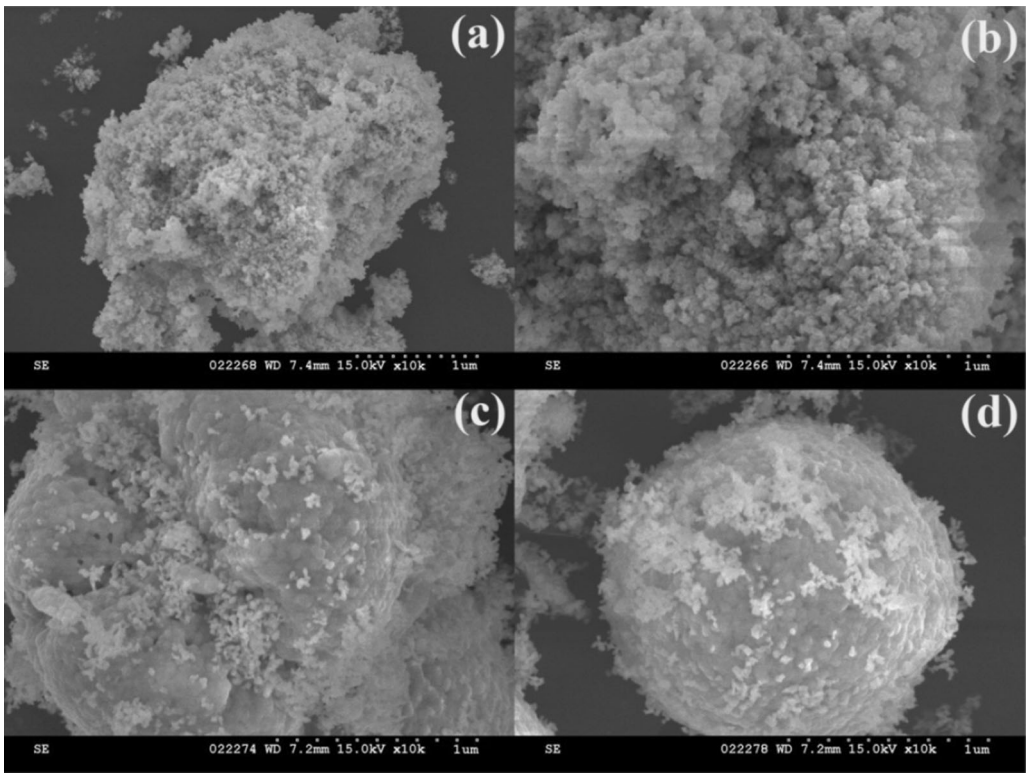

Figure 3. SEM images of (**a**) $SrWO_4$, (**b**) $SrWO_4$:HMTA, (**c**) $SrWO_4$:PVP and (**d**) $SrWO_4$:SDS materials.

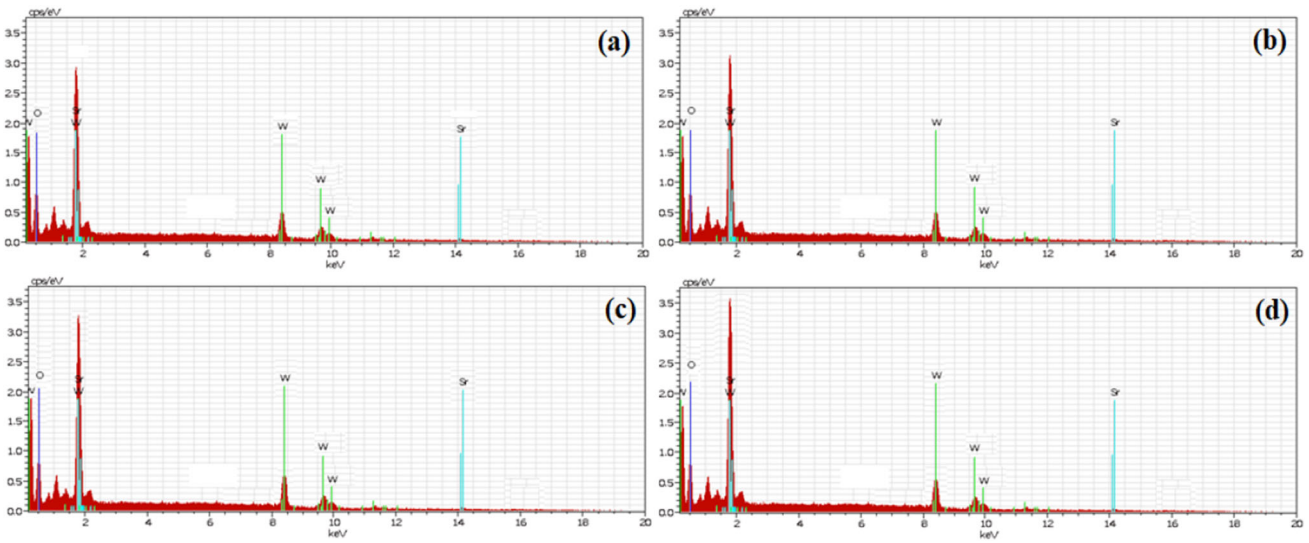

Figure 4. Energy-dispersive X-ray spectrometry spectra of (**a**) $SrWO_4$; (**b**) $SrWO_4$:HMTA; (**c**) $SrWO_4$:PVP and (**d**) $SrWO_4$:SDS materials.

(shown in table 1). Among all the samples, $SrWO_4$:SDS material exhibited more compressed unit cell than the other samples.

Figure 1c displays the growth mechanism of $SrWO_4$ particle in the presence of SDS. The surfactant SDS is composed of a negatively charged hydrophilic group and a hydrophobic carbon chain. When the SDS is mixed with water, number of micelles are produced and once it exceed their critical micelle concentration, uniformly distributed $SrWO_4$ particles were produced [25]. During the mixing of strontium nitrate, sodium tungstate and SDS solutions, Sr^{2+} and WO_4^{2-} ions attract each other leading to the formation

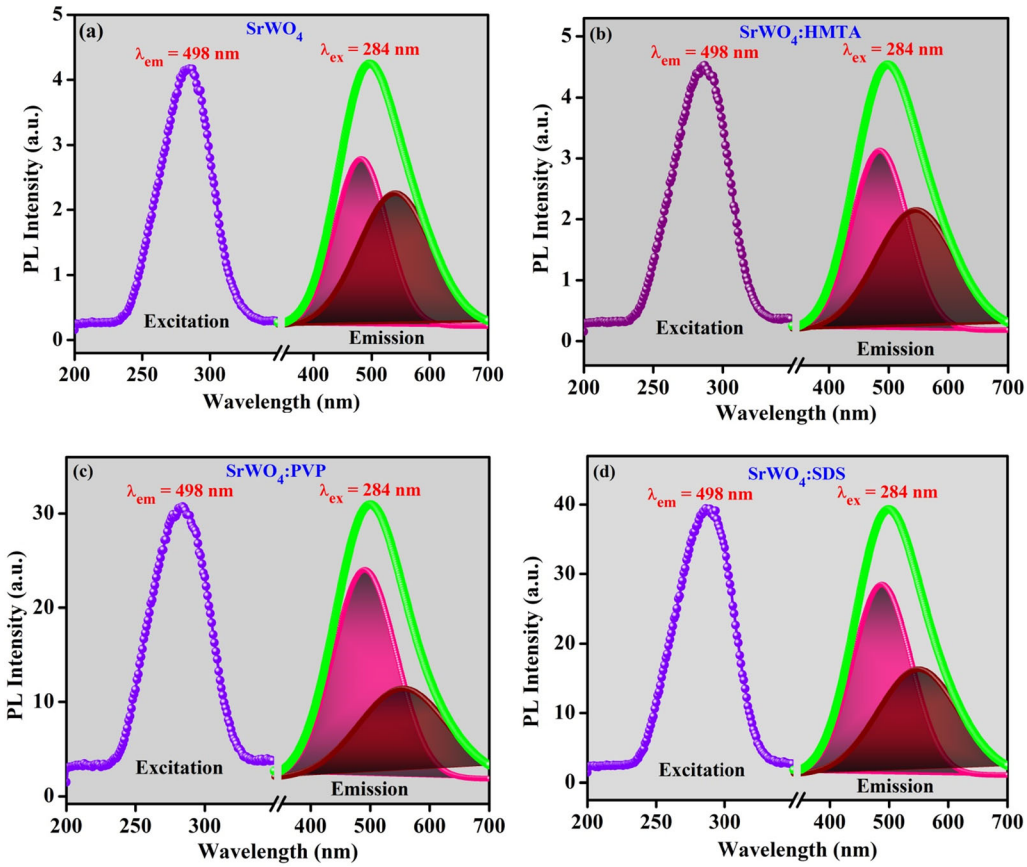

Figure 5. PL spectra of (**a**) $SrWO_4$, (**b**) $SrWO_4$:HMTA, (**c**) $SrWO_4$:PVP and (**d**) $SrWO_4$:SDS materials (from the centre break, the left spectrum is represented as the excitation peak, and the right-side spectrum is represented as the emission peak).

of $SrWO_4$. The micelle provides the adhesion between $SrWO_4$ molecules and as a result, uniform and monodispersed micron spheres were formed [25, 26].

The adhesion between $SrWO_4$ molecules is less in the case of PVP-assisted sample that can be attributed to the absence of tail end of the polymeric surfactant PVP, resulting in less crystallinity as indicated in PXRD of $SrWO_4$:PVP material (figure 1b). Similar XRD peaks were observed for $SrWO_4$:HMTA sample, which can be due to the fact that HMTA surfactant acts as a capping agent [27, 28]. During the reaction, HMTA helps to develop the particle growth at the capping level. But the possibility of static attraction of their surface group leads to the generation of uncapped particles that lowers the crystallinity and induces the agglomeration [29] (figure 3b).

The Scherrer equation [30] was used to calculate the average crystallite size of all the samples, which are about 19, 30, 36 and 56 nm for $SrWO_4$, $SrWO_4$:HMTA, $SrWO_4$:PVP and $SrWO_4$:SDS, respectively. The maximum crystallite size was obtained for $SrWO_4$:SDS due to their high crystallinity leading to less peak broadening of the X-ray diffraction peak [31–33].

In addition, detailed structural information of all the samples was investigated using the Rietveld refinement analysis. JANA 2006 software [34] was utilized for the refinement of observed PXRD, and the respective refined profiles are shown in figure 2a–d [34–36]. The packing diagram of $SrWO_4$ unit cell is shown in the inset of figure 2a–d. The structural parameters derived from the Rietveld analysis are summarized in table 1. The role of surfactant on the crystalline properties can be clearly identified from the unit cell parameters and crystallite size of the $SrWO_4$ material. The unit cell parameters obtained for $SrWO_4$:SDS materials are found to be low than other surfactant-assisted $SrWO_4$ materials.

3.2 *Morphology analysis*

Figure 3a–d shows the surface micrographs of the synthesized materials. The SEM image of surfactant-free $SrWO_4$ shows highly aggregated structure with unclear morphology. Likewise, $SrWO_4$:HMTA exhibited the agglomerated morphology that can be due to the maximum formation of uncapped nanoparticles [29]. On the other hand, $SrWO_4$:SDS sample showed a clear and spherical-shaped morphology in micrometre range, whereas partial spherical morphology was observed for $SrWO_4$:PVP. This

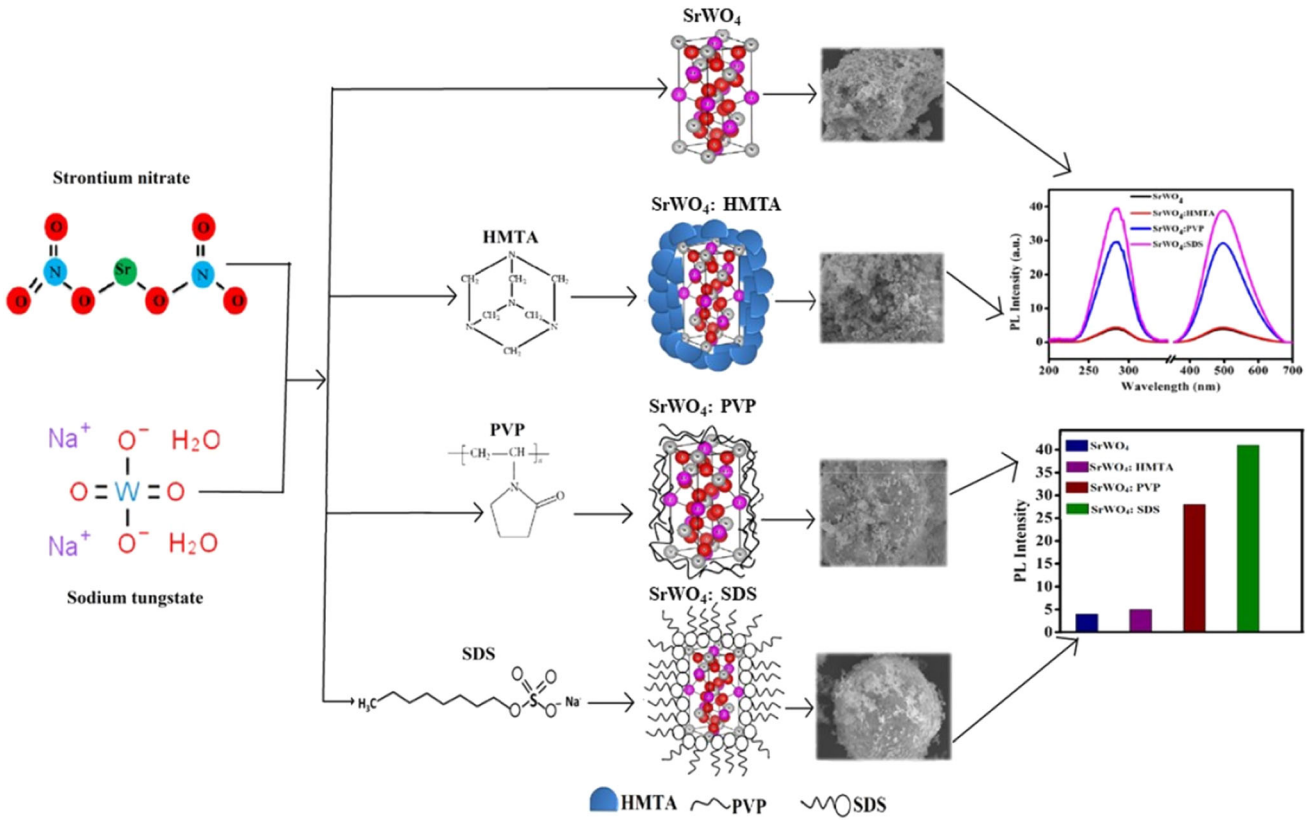

Figure 6. Schematic diagram showing the formation of surfactant-assisted $SrWO_4$ materials along with their morphology and PL intensity comparison.

observation is due to the phenomenon that during the reaction, the surfactant SDS controls the surface tension of the precipitated $SrWO_4$ suspension that stimulates the crystal growth direction and facilitates the uniform growth of crystals [37]. As a result, a narrow and highly intense X-ray diffraction peak (figure 1b) was observed revealing their high crystallinity with perfect spherical morphology. The crystallinity and surface morphology of phosphors significantly affect PL intensity and it is discussed in the PL analysis.

Energy-dispersive X-ray spectrometry measurement was carried out for all the $SrWO_4$ samples (figure 4a–d), which confirmed the presence of elements such as Sr, W and O in the prepared materials.

3.3 *PL analysis*

In general, $SrWO_4$ phosphor is reported to show remarkable PL behaviour without the presence of activator ions suggesting their self-activated photoluminescent property [38, 39]. The activator ion has intrinsic characteristics that will be used to create nonhomogenity in the host materials for inducing the optical properties of the materials. $SrWO_4$ host materials have existing self-luminescent centre that helps to emit light without adding any activator ions while

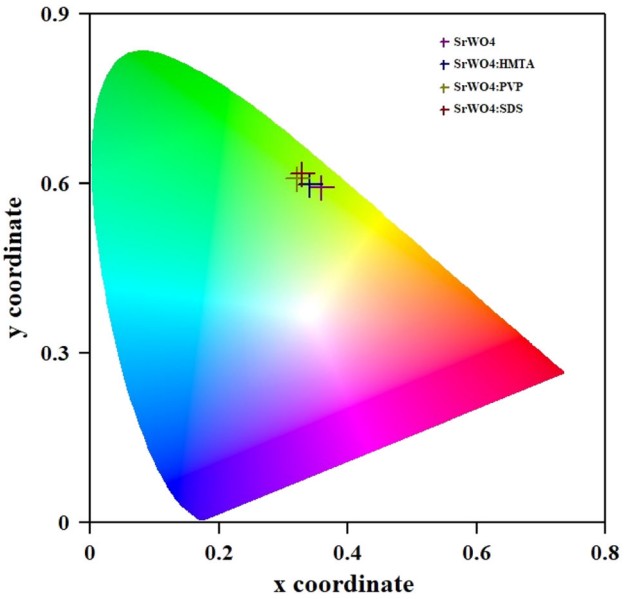

Figure 7. The Commission International de l'Eclairage chromaticity coordinates for as-prepared $SrWO_4$ materials.

excitation [40]. Furthermore, the luminescence behaviour of $SrWO_4$ materials can be enhanced by adding the surfactant during the preparation. The addition of surfactant influences the crystallinity and the morphology, resulting in the

Table 2. CIE values of $SrWO_4$ materials.

Sample	CIE coordinate	
	x	*y*
$SrWO_4$	0.359	0.594
$SrWO_4$:HMTA	0.341	0.598
$SrWO_4$:PVP	0.322	0.608
$SrWO_4$:SDS	0.329	0.618

enhancement of optical properties of the self-activated $SrWO_4$ phosphors.

In the present work, the effect of surfactants on the PL property of $SrWO_4$ phosphor was demonstrated and the respective excitation and emission spectra are shown in figure 5a–d. All the samples showed broad excitation in the wavelength range of 250–350 nm with a maximum value at 284 nm, while emission spectrum displays a broad peak in the wavelength range of 350–700 nm with a maximum peak value at 498 nm.

The reason for the luminescence behaviours of $SrWO_4$, $SrWO_4$:HMTA, $SrWO_4$:PVP and $SrWO_4$:SDS is due to the presence of structural defects that promotes electronic transition within the confined energy levels [41]. The tetrahedral matrix of the $SrWO_4$ contains a $[SrO_8]$ group, indicating 8 oxygen atoms are coordinated with Sr^{2+} cations forming a dodecahedral distorted geometry, while the matrix also contains a $[WO_4]$ group, implying 4 oxygen atoms enclosed in one tungsten atoms forming a tetrahedral geometry [13]. The emission of 498 nm green luminescence from the $SrWO_4$, $SrWO_4$:HMTA, $SrWO_4$:PVP and $SrWO_4$:SDS materials can be ascribed to $\left(WO_4^{2-}\right)$ lattice distortion of the tetrahedron symmetry [41] due to diverse angles between the O–W–O and the surface defects of the material. The broad emission peaks of all $SrWO_4$ materials are deconvoluted into two Gaussian curves. Primary emission around 490 nm showed pale green emission due to intrinsic emission from the WO_4^{2-} matrix functioning as luminescence centre. The secondary peak around 555 nm shows yellow emission corresponding to the presence of oxygen vacancies due to the deep lattice defects in the $SrWO_4$ matrix [17]. The high intensity of PL spectra is detected in $SrWO_4$:SDS materials, which are about 8 times higher than that of $SrWO_4$ and $SrWO_4$:HMTA samples. The effect of surfactant on the synthesis, and its influence on the morphology, along with the enhancement of the luminescent properties of the host materials are schematically represented in figure 6 for the clear understandings of the present work.

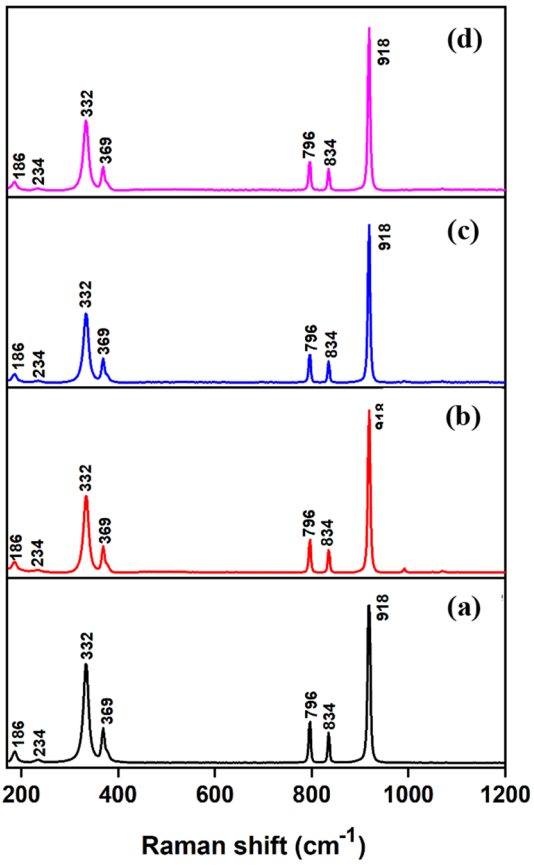

Figure 8. Raman spectra of (**a**) $SrWO_4$, (**b**) $SrWO_4$:HMTA, (**c**) $SrWO_4$:PVP and (**d**) $SrWO_4$:SDS samples.

The observed PL results in the present study are very much corroborated with the reported literature. Gupta *et al* [42] prepared $SrWO_4$ at different annealing temperatures, such as 300, 500, 700 and 900°C using the polyol method. They reported that the 490 nm PL emission was observed in $SrWO_4$ sample annealed at 700 and 900°C. In contrast, the 525 nm PL emission was observed in the $SrWO_4$ sample annealed at 300 and 500°C. They strongly suggested that the 490 nm emission of $SrWO_4$ is due to the electron–hole recombination between oxygen and tungsten in the WO_4^{2-} matrix. The 525 nm emission is attained due to the additional defect levels generated within the bandgap of the material. In the present study, the $SrWO_4$ was prepared by using surfactants and calcinated at 700°C. The ample calcination temperature and effective retardation of surface tension on the aqueous suspension performance of

Table 3. Assignment of Raman bands.

Raman shift (cm^{-1})	Peak assignment
186 234	Free rotation modes of WO_4^{2-}
332	W–O–W symmetric bending
369	W–O–W anti-symmetric bending
796 834	W–O anti-symmetric stretching
918	W–O symmetric stretching

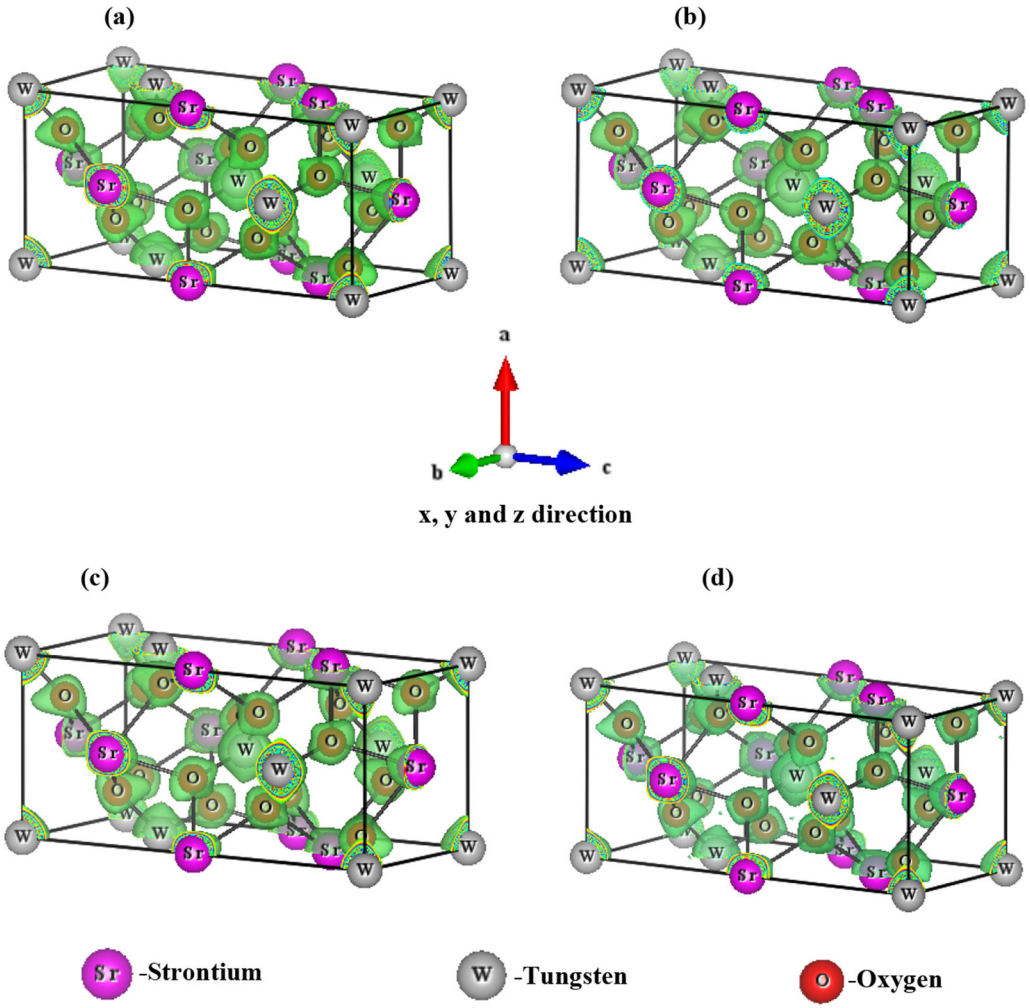

Figure 9. Three-dimensional electron density distribution of (**a**) $SrWO_4$, (**b**) $SrWO_4$:HMTA, (**c**) $SrWO_4$:PVP and (**d**) $SrWO_4$:SDS with iso-surface level 1.5 e $Å^{-3}$.

surfactant can develop the crystal growth and surface morphology that permits the better PL performance of as-prepared $SrWO_4$. Sun *et al* [43] synthesized $SrWO_4$ with different morphology such as nanoparticles, nanopeanuts and nanorods using the solvothermal-mediated microemulsion method. They reported that the 501 nm PL emission was observed in $SrWO_4$ nanoparticles and nanorods. But contrarily, the 468 nm emission was observed in $SrWO_4$ nanopeanuts. They suggested the distinct PL performance of nanopeanuts $SrWO_4$ is due to its surface roughness of nanopeanuts, which leads to the large surface-to-volume ratio that promotes the defects on the surface. The enhanced PL emission is due to uniformity in particle size and shape of phosphors. Uniform morphology can create more surface-related defect centres leading to high PL efficiency [44, 45]. In the present study, the clear spherical-shaped morphology was obtained in $SrWO_4$:SDS, which permits the more surface-related defect centres that enhance the PL intensity. Recently, Gao *et al* [38] synthesized $SrMoO_4$/$SrWO_4$ micro/nano heterojunction phosphor using the polyacrylamide gel method. They reported that the $SrMoO_4$/$SrWO_4$ heterojunction displays the 440 nm emission under 310 nm excitation. Similarly, $SrMoO_4$ and $SrWO_4$ phosphors prepared by the same method exhibit an ultraviolet emission peak at 378 nm and sky-blue emission at 465 nm, respectively. Their results suggested that the internal charge transfer of MoO_4 tetrahedron produces 378 nm UV emission and the lattice distortion of WO_4 tetrahedron makes 465 nm sky-blue emission. It is stated that the PL of $SrMoO_4$/$SrWO_4$ micro/nano heterojunction is due to the lattice distortion of $SrMoO_4$ and $SrWO_4$. Furthermore, their findings enunciated that the PL properties of $SrMoO_4$ and $SrWO_4$ are strongly dependent on the synthesis method. In the present study, $SrWO_4$ was prepared using the co-precipitation method, and surfactants were used to tune the crystallinity and surface morphology. The high crystallinity and clear spherical-shaped morphology were obtained in $SrWO_4$:SDS, which gives the high PL intensity. The high crystallinity and spherical morphology of $SrWO_4$:SDS favours the possibility of a less number of non-

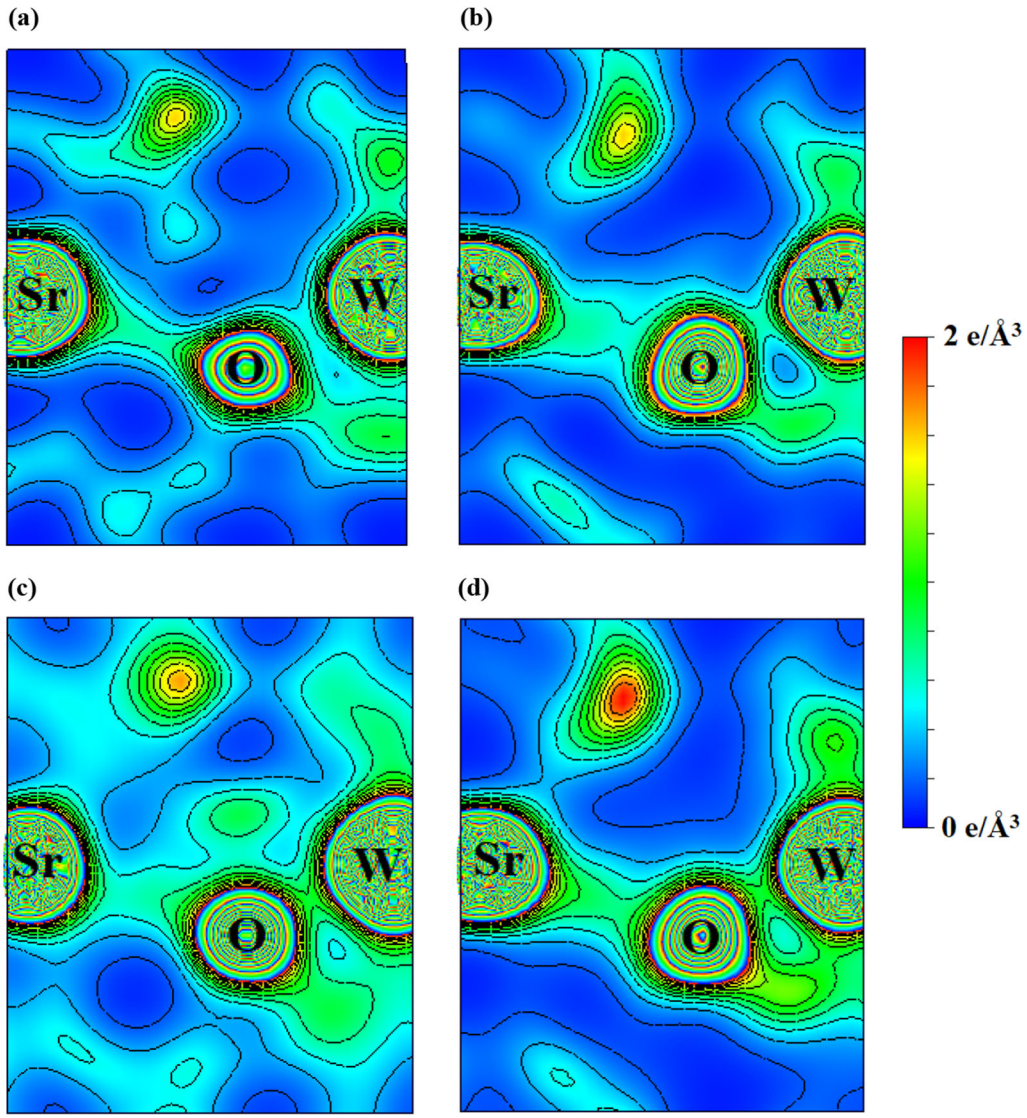

Figure 10. Two-dimensional electron density distribution maps of (204) plane in contour level 0–2 e $Å^{-3}$ with interval of 0.25 e $Å^{-3}$ of (**a**) $SrWO_4$ (**b**) $SrWO_4$:HMTA (**c**) $SrWO_4$:PVP and (**d**) $SrWO_4$:SDS.

radiative recombination process [7, 46, 47] in the WO_4^{2-} matrix, which improve the high PL intensity. The quantum yield of phosphor materials can be calculated based on the number of emitted photons with respect to the number of absorbed photons. In the present work, the quantum yield for $SrWO_4$:SDS could be higher than that of other samples because of their high emission intensity (see figure 5).

Figure 7 shows the Commission International de l'Eclairage (CIE) 1931 [48] chromaticity diagram of the $SrWO_4$ material with and without surfactant, which was obtained using GoCIE software. The calculated CIE parameters of all the $SrWO_4$ materials are given in table 2. From the table, it can be seen that the (x, y) projections of $SrWO_4$ and $SrWO_4$:HMTA are observed in the light green area, while $SrWO_4$:PVP and $SrWO_4$:SDS showing their projections in the intense green region than the other. From these results, it is revealed that the shift in the colour coordinates to the left suggests that $SrWO_4$:SDS materials are good candidates for solid-state lighting applications, especially in LED applications under UV excitation.

3.4 *Raman spectral studies*

Figure 8 shows the Raman spectral data obtained for $SrWO_4$ samples with and without surfactants. The measurements were performed in the spectral range of 170–1200 cm^{-1} at room temperature. All the samples show characteristic Raman peak corresponding to Scheelite-type $SrWO_4$ with tetragonal crystal structure. The spectrum has sharp intense peaks at 332, 369, 796, 834 and 918 cm^{-1}, and weak peaks at 186 and 234 cm^{-1}. There have been many literatures that

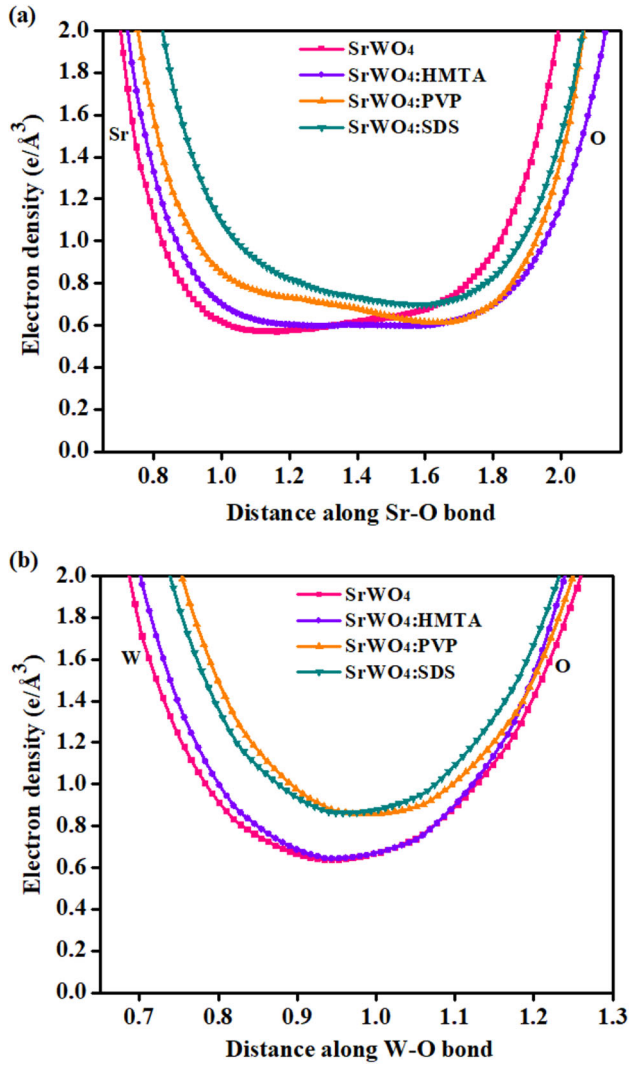

Figure 11. One-dimensional electron density distributions of $SrWO_4$ materials.

explain the Raman characteristics modes of $SrWO_4$ based on group theory calculations. As per the group theory, it has been explained that $SrWO_4$ by Scheelite-type tetragonal structure has 26 dissimilar vibrational active methods, including of Raman and Infra-red. Among the 26 modes, 13 are Raman active and the others are categorized as IR active modes, silent modes, acoustic modes and optic modes.

Out of 13 peaks, seven peaks were considered as internal ways and remaining six were external modes. Internal modes correspond to the vibrations of $[WO_4]^{2-}$ anionic group in the tetrahedron configuration of $SrWO_4$, while the external modes arise from the lattice phonon vibration of the Sr^{2+} cations in SrO_8 clusters with octahedral pattern and the rigid molecular anionic group. In this study, all the samples show seven internal Raman active vibrational modes, and the peaks assignments are shown in table 3. Generally, external modes of Raman peaks are observed in region >150 cm^{-1}. However, in the present study, those external mode peaks cannot be detected due to instrument spectral resolution limitation.

3.5 *Electron density distribution analysis*

The structural parameters extracted from the Rietveld profile refinement process were used to study the electron density distribution analysis [49, 50]. The maximum entropy method (MEM) [51–53] was employed for calculating the charge circulation between atoms of a tetragonal unit cell of $SrWO_4$ system through electron density distribution analysis. DYSNOMIA [54] and VESTA [55] software were used for the MEM calculations and visualization, respectively. In MEM, the unit cell is divided into the grid in $N_p = N_a \times N_b \times N_c$ pixels along the crystal axes *a*, *b* and *c* with a resolution of 1 e $Å^{-3}$ pixels. In this study, MEM computation was used to divide the unit cell into $64 \times 64 \times 144$ pixels. Figure 9a–d shows the tetragonal phase 3D charge density unit cell of all the $SrWO_4$ samples, which clearly visualized the spherical-shaped atoms of strontium, tungsten and oxygen packed in a single unit cell. The shaded light-green region surrounding all the atoms indicated the electron clouds. Figure 10 represents the 2D miller maps on (204) lattice planes drawn at the range 0 to 2 e $Å^{-3}$ with the interval of 0.25 e $Å^{-3}$. From figure 10d, it can be seen that the 2D map of $SrWO_4$:SDS sample exhibited more compressed contour lines between Sr–O and W–O atoms, which denoted that the maximum number of electrons were accumulated in the mid-bond valence region. The higher

Table 4. Bonding parameters of $SrWO_4$ materials.

	Sr–O		W–O	
Samples	Bond length (Å)	Mid-bond electron density (e $Å^{-3}$)	Bond length (Å)	Mid-bond electron density (e $Å^{-3}$)
$SrWO_4$	2.5831	0.5731	1.7873	0.6369
$SrWO_4$:HMTA	2.5837	0.5976	1.7810	0.6442
$SrWO_4$:PVP	2.5686	0.6126	1.7713	0.8569
$SrWO_4$:SDS	2.5599	0.6975	1.7703	0.8624

accumulation of contour lines leads to the maximum electron orientation that indicates the covalent nature possessed by Sr–O and W–O atoms. These observations are correlated with the high PL efficiency of $SrWO_4$:SDS material. Likewise, the cell constant values of the $SrWO_4$:SDS sample are low compared to the surfactant-free and the other two surfactant-assisted $SrWO_4$ materials. This indicates that the atoms are arranged at close distances within the unit cell of $SrWO_4$, which impact the lower bond length values between the atoms that expose the higher mid-bond electron densities of Sr–O and W–O. The charge accumulation and the bonding parameters are extracted for all the samples using 1D electron density profile. Figure 11a and b displays the 1D electron density profiles of the as-prepared $SrWO_4$ samples with and without surfactant. The bond length and electron density values obtained for the mid-bond of $SrWO_4$ materials are shown in table 4. Among all the samples, $SrWO_4$:SDS showed high electron density in the mid-bond region, confirming their enhanced PL emission characteristics. The good crystallinity and clear spherical-shaped morphology of $SrWO_4$:SDS lead to the better bonding and PL performance of the chosen material.

4. Conclusion

$SrWO_4$, $SrWO_4$:HMTA, $SrWO_4$:PVP and $SrWO_4$:SDS materials were prepared using co-precipitation method, and the samples were investigated to study the effect of surfactant on the structural, morphological and PL properties. X-ray diffraction investigation revealed pure tetragonal scheelite $SrWO_4$ materials. SEM measurements showed that among all the surfactants, $SrWO_4$:SDS material possess spherical-shaped morphology. The $SrWO_4$:SDS showed excellent PL performance with the emission of 498 nm under 284 nm excitation due to its high crystallinity and spherical-shaped morphology. From PL results, we conclude that the prepared SrWO4:SDS is the potential candidate for solid-state lighting applications.

Acknowledgements

We wish to thank the Kalasalingam Academy of Research and Education (KARE – Deemed to be University), International Research Centre (IRC) for providing the instrument utilities. We are grateful to Dr Arunachalam Lakshmanan, Director (R&D), Saveetha Engineering College, Chennai 602105, for PL measurements. We would also like to acknowledge Dr Naidu Dhanpal Jayram, Plasmonic Laboratory, Department of Physics, KARE, for utilizing the RAMAN characterization facility funded by SERB FILE NO.SRG/2019/001576. The author from KKU extend his appreciation to the Deanship of Scientific Research at KKU for funding to carry this work through the research groups program under Grant Number R.G.P. 2/147/43.

References

[1] Braden D R 2002 *Technol. Cult.* **43** 193
[2] Martinot E and Borg N 1998 *Energy Policy* **26** 1071
[3] Höppe H A 2009 *Angew. Chemie - Int. Ed.* **48** 3572
[4] Feldmann C, Jüstel T, Ronda C R and Schmidt P J 2003 *Adv. Funct. Mater.* **13** 511
[5] Lin Y C, Karlsson M and Bettinelli M 2016 *Top. Curr. Chem.* **374** 374
[6] Pereira P F S, Gouveia A F, Assis M, De Oliveira R C, Pinatti I M, Penha M *et al* 2018 *Phys. Chem. Chem. Phys.* **20** 1923
[7] Sivaganesh D, Saravanakumar S, Sivakumar V, Sasikumar S, Nandha Gopal J, Kalpana S *et al* 2020 *J. Mater. Sci. Mater. Electron.* **31** 8865
[8] Dai X J, Luo Y S, Zhang W D and Fu S Y 2010 *Dalt. Trans.* **39** 3426
[9] Sivakumar V, Sivaganesh D, Gopal J N, Muthuvinayagam M, Man J, Karthick P *et al* 2022 *Phys. B Phys. Condens. Matter* **644** 414155
[10] Thongtem T, Kungwankunakorn S, Kuntalue B, Phuruangrat A and Thongtem S 2010 *J. Alloys Compd.* **506** 475
[11] Liao J, Qiu B, Wen H, Chen J and You W 2009 *Mater. Res. Bull.* **44** 1863
[12] Zhang L, Bai Q, Wang L, Zhang A, Zhang Y and Xing Y 2014 Funct. *Mater. Lett.* **7** 2
[13] Dirany N, McRae E and Arab M 2017 *CrystEngComm.* **19** 5008
[14] Maheshwary R, Singh B P and Singh R A 2016 *Spectrochim. Acta - Part A Mol. Biomol. Spectrosc.* **152** 199
[15] Li L Z, Yan B, Lin L X and Zhao Y 2011 *J. Mater. Sci. Mater. Electron.* **22** 1040
[16] Tian G, Sheng N and Qiu X 2014 *Cryst. Res. Technol.* **49** 360
[17] Sivaganesh D, Saravanakumar S, Sivakumar V, Rajajeyaganthan R, Arunpandian M, Nandha Gopal J *et al* 2020 *Mater. Charact.* **159** 110035
[18] Lugo D M, Oberdisse J, Lapp A and Findenegg G H 2010 *J. Phys. Chem. B* **114** 4183
[19] Sakunthala A, Reddy M V, Selvasekarapandian S, Chowdari B V R and Selvin P C 2010 *J. Phys. Chem. C* **114** 8099
[20] Swathi S, Yuvakkumar R, Senthilkumar P, Ravi G and Velauthapillai D 2022 *Int. J. Hydrog. Energy* **47** 41984
[21] Patil S S, Mane R M, Khot K V, Mali S S, Kook Hong C and Bhosale P N 2021 *Sol. Energy* **220** 371
[22] Li Y, Zhou F, Zhu Z and Wu F 2019 *Appl. Surf. Sci.* **467** 819
[23] Saravanan R, Israel S, Swaminathan S, Kalidoss R and Muruganantham M 2002 *Cryst. Res. Technol.* **37** 1310
[24] Syed Ali K S, Saravanan R, Israel S, Açikgöz M and Arda L 2010 *Phys. B Condens. Matter* **405** 1763
[25] Xie S, Yuan M, Wang T, Liu J, Yan J, Li Z *et al* 2022 *Ceram. Int.* **48** 10113
[26] Li Z, Feng X, Mi L, Zheng J, Chen X and Chen W 2018 *Nano Res.* **11** 4038
[27] Gómez-Díaz D, Navaza J M and Rumbo A 2018 *J. Chem. Eng. Data* **63** 3846

[28] Rahman M Y A, Umar A A, Roza L and Salleh M M 2014 *Russ. J. Electrochem.* **50** 974
[29] Arun Kumar G, Bhojya Naik H S, Viswanath R, Suresh Gowda I K and Vinuth M 2017 *Mater. Today Proc.* **4** 3932
[30] Patterson A L 1939 *Phys. Rev.* **56** 978
[31] Wijesinghe S L, Mantilaka M M, Premalal V A, Herath M T, Mahalingam S, Edirisinghe M *et al* 2014 *Mater. Sci. Eng. C* **42** 83
[32] Modolon H B, Inocente J, Bernardin A M, Klegues Montedo O R and Arcaro S 2021 *Ceram. Int.* **47** 27685
[33] Nasiri-Tabrizi B 2014 *J. Adv. Ceram.* **3** 31
[34] Petrícek V, Dušek M and Palatinus L 2014 *Zeitschrift fur Krist.* **229** 345
[35] Rietveld H M 1969 *J. Appl. Crystallogr.* **2** 65
[36] Rietveld H M 2014 *Phys. Scr.* **89** 098002
[37] Yan Y, Wang J, Hojamberdiev M, Lu Z, Ren B and Xu Y 2014 *J. Alloys Compd.* **597** 282
[38] Gao H, Yu C, Wang Y, Wang S, Yang F, Tang S *et al* 2022 *J. Lumin.* **243** 118660
[39] Gao H, Wang Y, Gao Q, Pan X, Wang S, Yang H *et al* 2021 *Optik* **241** 167040
[40] Ju G, Hu Y, Chen L, Jin Y, Zhang S, Xue F *et al* 2016 *Mater. Res. Bull.* **83** 211
[41] Sczancoski J C, Avansi W, Costa G S, Siu Li M, Mastelaro V R, Santos R S *et al* 2015 *J. Mater. Sci.* **50** 8089
[42] Gupta S K, Sudarshan K, Ghosh P S, Sanyal K, Srivastava A P, Arya A *et al* 2016 *RSC Adv.* **6** 3792
[43] Sun L, Guo Q, Wu X, Luo S, Pan W, Huang K *et al* 2007 *J. Phys. Chem. C* **111** 532
[44] Crapanzano R, Villa I, Mostoni S, D'arienzo M, Di Credico B, Fasoli M *et al* 2020 *Nanomaterials* **10** 1
[45] Manoharan D, Loganathan A, Kurapati V and Nesamony V J 2015 *Ultrason. Sonochem.* **23** 174
[46] Blasse G and Grabmaier B C 1994 A general introduction to luminescent materials. Springer, Berlin
[47] Sivaganesh D, Saravanakumar S, Sivakumar V, Sasikumar S, NandhaGopal J and Ramanathan R 2021 *Luminescence* **36** 99
[48] Sasikumar S, Saravanan R, Saravanakumar S and Aravinth K 2017 *J. Mater. Sci. Mater. Electron.* **28** 9950
[49] Saravanan R, Syed Ali K S and Israel S 2008 *Pramana - J. Phys.* **70** 679
[50] Saravanakumar S, Sivaganesh D, Sivakumar V, Sasikumar S, Thirumalaisamy T K, Sayed M A *et al* 2021 *Phys. Scr.* **96** 125817
[51] Saravanakumar S, Saravanan R and Sasikumar S 2014 *Chem. Pap.* **68** 788
[52] Saravanakumar S, Sivaganesh D, Sivakumar V, Yang L, Rajajeyaganthan R and Israel S 2022 *Optik* **249** 168169
[53] Sivaganesh D, Saravanakumar S, Sivakumar V, Sangeetha R, Berchmans L J, Syed Ali K S *et al* 2021 *J. Mater. Sci. Mater. Electron.* **32** 1466
[54] Momma K, Ikeda T, Belik A A and Izumi F 2013 *Powder Diffr.* **28** 184
[55] Momma K and Izumi F 2011 *J. Appl. Crystallogr.* **44** 1272